Development of optical hyperlens for imaging below the diffraction limit

Hyesog Lee, Zhaowei Liu, Yi Xiong, Cheng Sun and Xiang Zhang*

5130 Etcheverry Hall, NSF Nanoscale Science and Engineering Center (NSEC), University of California, Berkeley, CA 94720
*Corresponding author: xiang@berkeley.edu
http://xlab.me.berkeley.edu

Abstract: We report here the design, fabrication and characterization of optical hyperlens that can image sub-diffraction-limited objects in the far field. The hyperlens is based on an artificial anisotropic metamaterial with carefully designed hyperbolic dispersion. We successfully designed and fabricated such a metamaterial hyperlens composed of curved silver/alumina multilayers. Experimental results demonstrate far-field imaging with resolution down to 125nm at 365nm working wavelength which is below the diffraction limit.

OCIS codes: (110 0180) Microscopy; (220.4241) Optical design and fabrication: Nanostructure fabrication

---

References and links

1. E. Abbe, Arch. Mikroskop. Anat. **9**, 413 (1873)
2. E. Betzig, J. K. Trautman, T. D. Harris, J. S. Weiner and R. L. Kostelak, "Breaking the diffraction barrier – optical microscopy on a nanometric scale," Science **251**, 1468-1470 (1991)
3. S. W. Hell, "Toward Fluorescence nanoscopy," Nat. Biotechnol. **21**, 1347-1355 (2003)
4. M. G. L. Gustafsson, "Nonlinear structured-illumination microscopy: Wide-field fluorescence imaging with theoretically unlimited resolution," P. Natl. Acad. Sci. **102,** 13081-13086 (2005)
5. J. B. Pendry, "Negative refraction makes a perfect lens," Phys. Rev. Lett. **85**, 3966-3969 (2000)
6. N. Fang, H. Lee, C. Sun and X. Zhang, "Sub-Diffraction-Limited Optical Imaging with a Silver Superlens" Science **308**, 534-537 (2005)
7. H. Lee, Y. Xiong, N. Fang, W. Srituravanich, S. Durant, M. Ambati, C. Sun and X. Zhang, "Realization of optical superlens imaging below the diffraction limit," New J. Phys. **7**, 255 (2005)
8. D. Melville, R. Blaikie, "Super-resolution imaging through a planar silver layer," Opt. Express. **13**, 2127-2134 (2005)
9. T. Taubner, D. Korobkin, Y. Urzhumov, G. Shvets, R. Hillenbrand, "Near-Field microscopy Through a SiC Superlens," Science **313**,1595 (2006)
10. V. Podolskiy, E. E. Narimanov, "Near-sighted superlens," Opt. Lett. **30**, 75-77 (2005)
11. S. Durant, Z. Liu, J. Steele, X. Zhang, "Theory of the transmission properties of an optical far-field superlens for imaging beyond the diffraction limit," J. Opt. Soc. Am. B. **23**, 2383-2392 (2006)
12. Z. Liu, S. Durant, H. Lee, Y. Pikus, N. Fang, Y. Xiong, C. Sun and X. Zhang, "Far-Field Optical Superlens," Nano Lett. **7,** 403-408 (2007)
13. Z. Liu, S. Durant, H. Lee, Y. Pikus, Y. Xiong, C. Sun and X. Zhang, "Experimental studies of far-field superlens for sub-diffractional optical imaging," Opt. Express **15**, 6947-6954 (2007)
14. Y. Xiong, Z. Liu, C. Sun, and X. Zhang, "Two-dimensional imaging by far-field superlens at visible wavelengths," Nano Lett. (Web Release Date: 05-Oct-2007)
15. J. B. Pendry and S. A. Ramakrishna, "Near-field lenses in two dimensions," J. Phys. Condens. Matter **14**, 8463-8479 (2002)
16. J. B. Pendry, "Perfect Cylindrical lenses," Opt. Express **11**, 755-760 (2003)
17. Z. Jacob, L. V. Alekseyev and E. Narimanov, "Optical hyperlens: Far-field imaging beyond the diffraction limit," Opt. Express **14**, 8247-8256 (2006)
18. A. Salandrino and N. Engheta, "Far-field subdiffraction optical microscopy using metamaterial crystals: Theory and simulations," Phy. Rev. B **74**, 075103 (2006)
19. Z. Liu, H. Lee, Y. Xiong, C. Sun and X. Zhang, "Far-Field Optical Hyperlens Magnifying Sub-Diffraction-Limited Objects," Science, **315**, 1686 (2007)

20. VA Podolskiy and EE Narimanov "Strongly anisotropic waveguide as a nonmagnetic left-handed system," Phys. Rev. B **71**, 201101 (2005)
21. VA Podolskiy, L Alekseyev and EE Narimanov, "Strongly anisotropic media: the THz perspectives of left-handed materials," J. Mod. Opt. **52**, 2343 (2005)
22. R. Wangberg, J. Elser, E. E. Narimanov and V. A. Podolskiy, "Non-magnetic nano-composites for optical and infrared negative refraction index media," J. Opt. Soc. Am. B. **23**, 498 (2006)
23. P. B. Johnson and R. W. Christy, "Optical Constants of the Noble Metals," Phys. Rev. B **6**, 4370-4379 (1972)
24. E. D. Palik, Handbook of Optical Constants of Solids (1995)

1. Introduction

Ever since Abbe's discovery in 1873[1], the "diffraction limit" in far-field optical imaging was considered to be a fundamental barrier. Since high spatial frequency information carried by evanescent waves only exists in the near field of an object, only the propagating light reaches the far-field image plane and the resolution of any conventional microscope is limited to approximately half of the wavelength. Collecting the evanescent information directly in the near field has long been considered as the most straightforward and effective way to overcome the diffraction barrier. Near-field scanning optical microscope (NSOM) brings a sharp tip down to the near field of an object [2]. The evanescent information is then brought to the far field and the image is electronically reconstructed. Non-linear optical effects are utilized in fluorescent microscopy. In stimulated emission depletion (STED) microscopy, the scanning spot size can be significantly reduced by spatially controlled stimulated quenching of excited fluorescent molecules [3]. Structured illumination microscopy utilizes periodic lines or dot arrays to illuminate an object and sub-diffraction-limited images can be reconstructed numerically from a series of measurements based on moiré fringe concept [4]. Despite the success of aforementioned techniques, the scanning and the image reconstruction methods have the major drawback of being slow which is un-suitable for real-time imaging, in addition to the need of complex optics and non-linear materials.

A new imaging concept called superlensing received much attention for its ability to restore evanescent waves and project sub-diffraction-limited images without scanning [5]. Decaying evanescent field is amplified by a negative index material and the concept was validated experimentally by using a thin slab of silver [6-8] and SiC [9]. Even though it was pointed out that the superlensing was 'near-sighted' [10], the demonstration of this near-field superlensing raised the hope of developing a far-field superlens(FSL) which is capable of imaging in comparable resolution even in the far field [11-13]. A proof-of-concept experiment has been reported that sub-diffraction-limited resolution up to 120nm was achieved using a FSL [12, 13, 14].

In this paper, we describe an experimental realization of a new sub-diffraction-limit imaging method called 'hyperlens imaging'. Similar to the geometry of cylindrical superlens [15, 16], a hyperlens takes a form of cylindrical metamaterial comprising periodic metal and dielectric layers. This anisotropic metamaterial has electric permittivities in opposite signs in two orthogonal directions, which not only enables waves with large tangential wave vectors to propagate in the medium but also achieves an image magnification [17, 18]. We reported 150nm resolution which is beyond the diffraction limit of conventional microscopes [19]. Here we give detailed account of the hyperlens design, structure fabrication, and imaging experiments as well as a new result of an improved resolution.

2. Hyperlens Theory and Design

The hyperlens theory is briefly summarized in Fig. 1. The dispersion of electromagnetic(EM) wave is represented by $\frac{k_r^2}{\varepsilon_\theta} + \frac{k_\theta^2}{\varepsilon_r} = \frac{\omega^2}{c^2}$ in cylindrical coordinates, where k_r and k_θ are wave vectors, ε_r and ε_θ are permittivities in radial and tangential directions respectively, ω is the

angular frequency, and c is the speed of light. Figure 1(a) shows isofrequency contours in k-space in which isotropic medium has circular dispersion (red). The accessible range of k_θ, which determines the imaging resolution, is limited to the radius of the circle, $r = \varepsilon^{1/2} = n$, where n is the refractive index. Higher index materials are sought to be used in immersion microscopy for this reason, but there's limited availability in nature – commonly used immersion oil gives n only around 1.5. However, it was shown that a material with anisotropic electrical responses in two orthogonal tensor components can indeed support the propagation of EM waves with large wave vectors [20, 21, 22]. In case of $\varepsilon_r < 0$ and $\varepsilon_\theta > 0$, hyperbolic
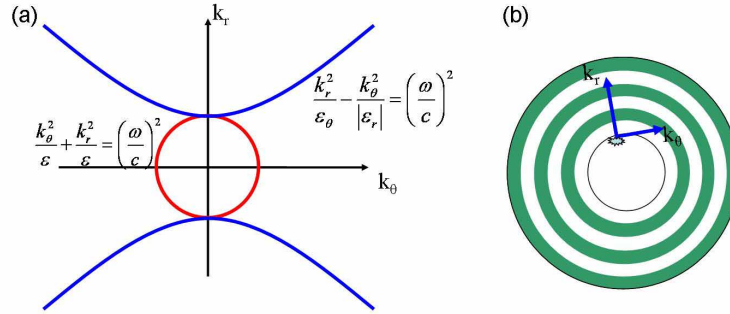

Fig. 1. Working principle of hyperlens. (a) Red circle: dispersion isofrequency curve of light in isotropic medium in cylindrical coordinate. Blue curve: hyperbolic dispersion in an anisotropic medium when $\varepsilon_r < 0$ and $\varepsilon_\theta > 0$ (b) One suggested cylindrical hyperlens structure. Multi-concentric layers of alternating metal and dielectric layers make anisotropic metamaterial.

isofrequency contour is achieved (blue) and waves with larger k_θ that are commonly evanescent become propagating (other combinations of permittivity values can result in different dispersion characteristics).

Such a medium can be realized using the metamaterial concept. Figure 1(b) shows one exampled structure which consists of thin alternating layers of a metal and a dielectric [15]. Since metals tend to have $\varepsilon_m < 0$ and dielectrics have $\varepsilon_d > 0$ in the visible frequency range, a metamaterial which contains both of the materials can be designed to exhibit opposite signs of permittivity in two orthogonal directions. When a small object is placed at the center of such a cylindrical 'hyperlens' (Fig.1(b)), the object scatters the light and generates a wide band of k_θ. As large wave vectors propagate along the radial direction, the k_θ component gradually becomes smaller due to the conservation of angular momentum. The fine feature information of an object is then brought to far field magnified which can be imaged directly by conventional optics.

In designing a realizable hyperlens, the permittivity of the metal(ε_m) and the dielectric(ε_d) have to match in such a way that the metamaterial has desired anisotropic characteristic, and each layer thickness must be much smaller than the wavelength to be treated as an effective medium. In addition, the structure parameters need to be within the capability of currently available nano-fabrication techniques.

For this experiment, Silver (Ag)($\varepsilon_m = -2.4012 + 0.2488i$ [23]) and Aluminum Oxide (Al$_2$O$_3$)($\varepsilon_d = 3.217$ [24]) were used and the effective permittivity of the designed metamaterial was calculated using $\varepsilon_\theta = p\varepsilon_m + (1-p)\varepsilon_d$, $\varepsilon_r = \dfrac{\varepsilon_m \varepsilon_d}{(1-p)\varepsilon_m + p\varepsilon_d}$, where p is the filling ratio of the metal. At 365nm working wavelength with $p = 0.5$, hyperbolic dispersion is obtained as shown in Fig. 2(a).
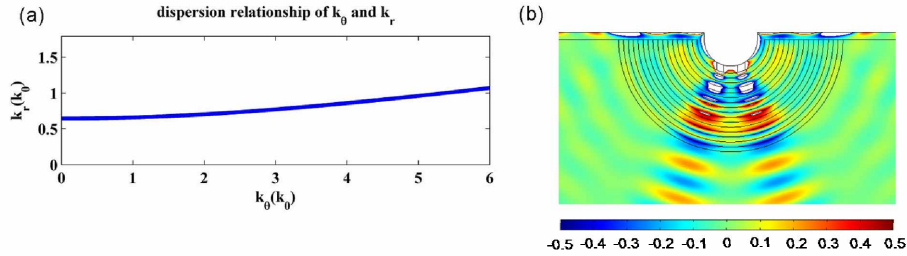
Fig. 2. Hyperlens designed for experiment. (a) Isofrequency contour of the designed metamaterial structure. k_r and k_θ are normalized to $k_0 = 2\pi/365nm$ (b) Simulated magnetic field distribution. The hyperlens consists of 8 pairs of Ag (35nm)/ Al$_2$O$_3$ (35nm) layers on a curved quartz mold. The two line objects (150nm separation through 50nm Cr film) are gradually magnified along the radial direction under p-polarized 365nm light illumination.

COMSOL Multiphysics$^{\text{TM}}$ 3.3 was used to simulate the performance of the designed hyperlens, and its cross section is shown in Fig. 2(b). The thickness of each layer was set to 35nm after considering both the applicability of the effective medium approximation and the acceptable film quality achievable in fabrication. The surrounding material is quartz ($\varepsilon_{qtz} = 2.174$) and the overall dimension is close to that of our fabricated hyperlens in which two 50nm wide openings with 150nm separation in a 50nm thick Cr layer serve as objects. With a p-polarized (electric field perpendicular to the groove direction) 365nm illumination from the top, it is clearly shown that the magnified image is formed by the hyperlens just outside the structure and its propagating property assures that the image is sent to the far field. The magnification, determined by the ratio of outer(r_o) and inner(r_i) radius, r_0/r_i, is estimated to be $800nm/240nm \approx 3.3$, which agrees well with the simulation result. The 16 layer design is to obtain a reasonable transmission through the structure during the image detection, but a larger magnification can be obtained with more layers.
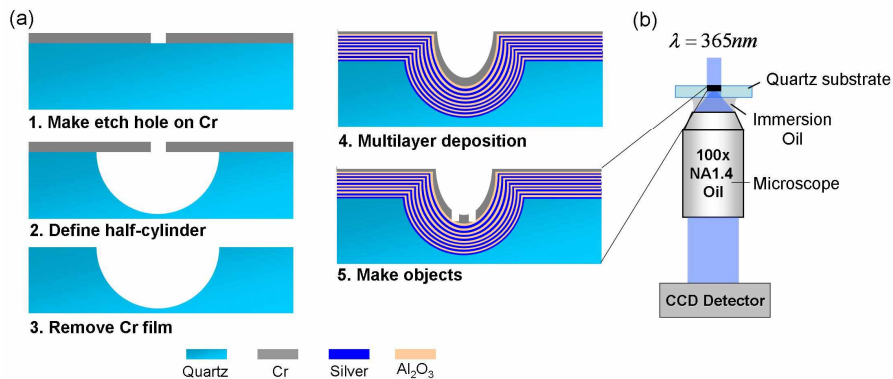

Fig. 3. (a) Hyperlens sample fabrication process flow. Through the etch hole on a Cr film (1), isotropic wet etching makes cylindrical groove in quartz (2). After Cr film is removed (3), multilayer hyperlens structure is fabricated using alternate deposition of Ag and Al$_2$O$_3$ (4). A Cr film caps the hyperlens structure for object fabrication (5). (b) Imaging setup. Completed hyperlens/object sample is placed under objective with incident light at 365nm, conventional far field microscope with 100X oil immersion objective and UV sensitive CCD detector was used for direct far field imaging.

3. Fabrication and Characterization

The fabrication process of our hyperlens is shown in Fig. 3(a). A thin Cr layer (150nm) was deposited on a quartz wafer (150μm thick) by an electron beam evaporation process(EB3, BOC Edwards). Then, a 50nm wide etch slit was made using Focused Ion Beam (FIB, STRATA 201XP, FEI) and the half-cylindrical groove was defined through isotropic wet etching of quartz in Buffered Oxide Etch (BOE) solution of 10:1 dilution ratio. In 12minutes, groove diameter of approximately 1.6μm was achieved. The RMS (Root Mean Squared) surface roughness of the groove was measured to be 1.3nm by Atomic Force Microscopy (Dimension 3100, Veeco). Since multiple Ag and Al_2O_3 thin films were to be deposited, the initial surface quality was a crucial factor in achieving tolerable smoothness of subsequent layers. The Cr layer was removed by another wet-etching step (CR-7 Cr etchant), and the multilayer structure was deposited at a low pre-deposition pressure of 3μTorr to ensure the best possible surface quality of each layer. Starting from the Ag layer, Al_2O_3 and Ag films were deposited alternatively at 0.3nm/s, and a 50nm of Cr film was deposited on top of the 16th layer (Al_2O_3). Despite the directional nature of electron beam evaporation deposition, a reasonably good side-wall coverage was achieved(Fig. 4). Finally, various objects were inscribed on the Cr film by FIB.
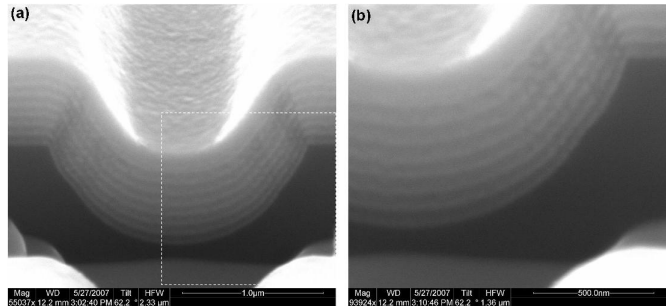

Fig. 4. A SEM picture of the cross section of a hyperlens structure. A hyperlens without any fabricated object was cut using FIB. (a) 16 Ag/Al_2O_3 layers are clearly shown, bright and dark layers are Ag and Al_2O_3 respectively. The top thick and bright layer is Chromium. Even with directional E-beam evaporation deposition method, side wall coverage is close to conformal due to low deposition rate. (b) Zoom-in picture of white square in (a).

Figure 3(b) shows the schematic of our hyperlens imaging setup. The fabricated sample was measured using an inverted optical microscope (Axiovert mat 200, 100x oil immersion objective, N.A.=1.4, Zeiss). The object was illuminated by a mercury lamp (HBO, Zeiss) with a band pass filter (centered at wavelength of 365nm and bandwidth of 10nm) and a UV polarizer. The magnified image was then captured by a UV sensitive TE-cooled CCD camera (VersArray 1300F, Princeton Instruments) with 20 seconds of exposure time. In order to find the right focus plane for the image, a step-motor (VEXTA RK series 5-phase stepping motor) was installed to the fine focusing knob of the microscope and the Z-focusing is scanned in 50nm step.

4. Imaging Results and Discussion

Figure 5(a) is a top-view scanning electron microscope (SEM) picture of a line pair object with center-to-center distance of 130nm and line width of ~50nm. They were placed off the center(Fig.5(a)) to show that an object can be placed anywhere in the groove to be imaged with good resolution and negligible position-dependant distortions.

The smallest distance (Δ) that can be resolved by the transmission mode imaging setup is estimated to be about 260nm from a simple equation: $\Delta = \lambda / NA$ where, $\lambda = 365nm$, and NA (Numerical Aperture)=1.4. Nevertheless, the 130nm distance object is clearly resolved through the hyperlens as shown in Fig. 5(b). The center-to-center distance of the enlarged image is about 300nm which represents the magnification of about 2. This is lower than the
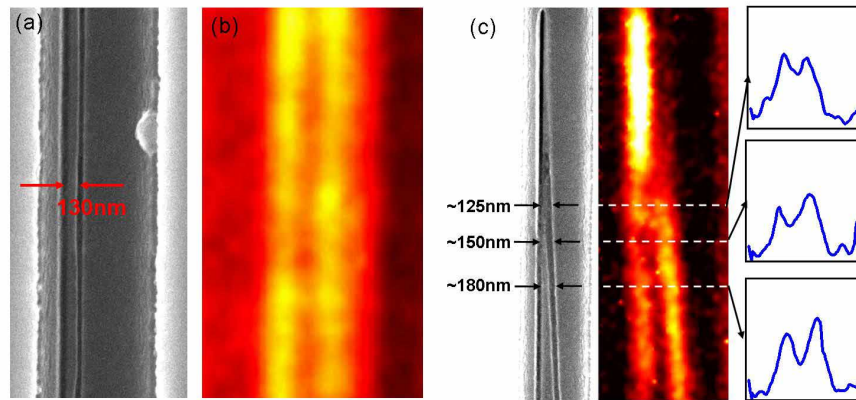
Fig. 5. Hyeperlens imaging results. (a) SEM image of 130nm line pair object on Cr film. Dark region is the hyperlens and the bright region is the flat surface. (b) Image captured by optical microscope through hyperlensing shows 130nm gap is clearly resolved. (c) Left: SEM image of tilted line pair object with indicated gap sizes. Middle: Image captured by optical microscope through hyperlensing. Right: Intensity profiles of the three indicated cross sections showing resolved 125nm gap (top).

predicted value of 3.3, which can be attributed to the imperfect concentricity of the fabricated structure. The non-ideal sample conditions such as surface and interface scattering also affected the experimental transmission coefficient which is about one order smaller than predicted by simulation. Obviously, the transmission level directly affects the exposure time of detection which is essential for high speed imaging. Nevertheless, it is possible to realize optical hyperlenses for true real-time imaging utilizing currently available materials and nanofabrication techniques.

Figure 5(c) shows the imaging results of a tilted line pair object which was designed to measure the resolution limit of our hyperlens. The intensity cross section revealed that our hyperlens was able to resolve down to 125nm which is more than a two-fold resolution improvement. In principle, the resolving power of a hyperlens is only limited by its geometry and thus the fabrication imperfections. However, the metamaterial still has a cut-off wave vector even at an acceptable transmission due to the inevitable material loss which sets the practical resolution limit. It is worth mentioning that the hyperlens we demonstrated here is able to magnify only in horizontal direction because of its cylindrical geometry. However, spherical shape can be designed and fabricated in the same way, which will be able to magnify in all planar directions to achieve true two-dimensional(2D) nano-optical imaging. This work is on-going and will be reported elsewhere.

5. Conclusion

This work provides the detailed accounts of the design, fabrication and characterization of the optical hyperlens. The demonstrated hyperlens, which is a metamaterial with concentric multilayers of metal and dielectric, utilizes its unusual anisotropic characteristic to directly transfer sub-wavelength information to the far field. Combining hyperlens with an optical microscope, a sub-diffraction-limited imaging was demonstrated with 125nm resolution. Hyperlensing opened new and exciting possibilities for real-time nanoscale optical imaging.

Acknowledgements